



3D Printing of Drug-Loaded Thermoplastic Polyurethane Meshes: A Potential Material for Soft Tissue Reinforcement in Vaginal Surgery

Dominguez-Robles, J., Mancinelli, C., Mancuso, E., Garcia-Romero, I., Gilmore, B. F., Casettari, L., Larraneta, E., & Lamprou, D. (2020). 3D Printing of Drug-Loaded Thermoplastic Polyurethane Meshes: A Potential Material for Soft Tissue Reinforcement in Vaginal Surgery. *Pharmaceutics*, 12(1), Article 63.
<https://doi.org/10.3390/pharmaceutics12010063>

[Link to publication record in Ulster University Research Portal](#)

Published in:
Pharmaceutics

Publication Status:
Published (in print/issue): 13/01/2020

DOI:
[10.3390/pharmaceutics12010063](https://doi.org/10.3390/pharmaceutics12010063)

Document Version
Author Accepted version

General rights
Copyright for the publications made accessible via Ulster University's Research Portal is retained by the author(s) and / or other copyright owners and it is a condition of accessing these publications that users recognise and abide by the legal requirements associated with these rights.

Take down policy
The Research Portal is Ulster University's institutional repository that provides access to Ulster's research outputs. Every effort has been made to ensure that content in the Research Portal does not infringe any person's rights, or applicable UK laws. If you discover content in the Research Portal that you believe breaches copyright or violates any law, please contact pure-support@ulster.ac.uk.

1 Article

2 3D printing of drug-loaded thermoplastic 3 polyurethane meshes: A potential material for soft 4 tissue reinforcement in vaginal surgery

5 Juan Domínguez-Robles ^{1,†}, Caterina Mancinelli ^{1,2,†}, Elena Mancuso ³, Inmaculada García-
6 Romero ⁴, Brendan F. Gilmore ¹, Luca Casettari ², Eneko Larrañeta ^{1,*}, Dimitrios A. Lamprou ^{1,*}

7 ¹ School of Pharmacy, Queen's University Belfast, 97 Lisburn Road, Belfast BT9 7BL, UK;

8 j.dominguezrobles@qub.ac.uk (J.D.-R.); b.gilmore@qub.ac.uk (B.F.G.)

9 ² Department of Biomolecular Sciences, University of Urbino Carlo Bo, Piazza del Rinascimento, 6, 61029

10 Urbino, PU, Italy; c.mancinelli3@campus.uniurb.it (C.M.); luca.casettari@uniurb.it (L.C.)

11 ³ Nanotechnology and Integrated Bio-Engineering Centre (NIBEC), Ulster University, Jordanstown Campus
12 BT37 0QB, UK; e.mancuso@ulster.ac.uk (E.M.)

13 ⁴ Wellcome-Wolfson Institute for Experimental Medicine, Queen's University Belfast, Belfast, BT9 7BL, UK;
14 I.Garcia-Romero@qub.ac.uk (I.G.-R.)

15 * Correspondence: e.larraneta@qub.ac.uk (E.L.); d.lamprou@qub.ac.uk (D.A.L.)

16 † These authors contributed equally to this work.

17 Received: date; Accepted: date; Published: date

18 **Abstract:** Current strategies to treat pelvic organ prolapse (POP) or stress urinary incontinence
19 (SUI), include the surgical implantation of vaginal meshes. Recently, there has been multiple reports
20 of issues generated by these meshes conventionally made of poly(propylene). This material is not
21 the ideal candidate due to its mechanical properties leading to complications such as chronic pain
22 and infection. In the present manuscript, we propose the use of an alternative material,
23 thermoplastic polyurethane (TPU), loaded with an antibiotic in combination with fused deposition
24 modelling (FDM) to prepare safer vaginal meshes. For this purpose, TPU filaments containing
25 levofloxacin (LFX) in various concentrations (e.g., 0.25, 0.5, and 1%) were produced by extrusion.
26 These filaments were used to 3D print vaginal meshes. The printed meshes were fully characterized
27 through different test/analysis such as fracture force studies, attenuated total reflection-Fourier
28 transform infrared, thermal analysis, scanning electron microscopy, X-ray microcomputed
29 tomography (μ CT), release studies and microbiology testing. The results showed that LFX was
30 uniformly distributed within the TPU matrix, regardless the concentration loaded. The mechanical
31 properties showed that poly(propylene) (PP) is a tougher material with lower elasticity than TPU
32 which seemed to be a more suitable material due to its elasticity. In addition, the printed meshes
33 showed a significant bacteriostatic activity on both *Staphylococcus aureus* and *Escherichia coli* cultures
34 minimising the risk of infection after implanting them. Therefore, the incorporation of LFX to the
35 TPU matrix can be used to prepare anti-infective vaginal meshes with enhanced mechanical
36 properties compared with current PP vaginal meshes.

37 **Keywords:** 3D printing; fused deposition modeling; extrusion; vaginal meshes; mechanical
38 properties; drug release, anti-infective devices; pelvic organ prolapse; stress urinary incontinence

39 1. Introduction

40 Pelvic organ prolapse (POP) and stress urinary incontinence (SUI), are two very common
41 disorders affecting 30-40% of women worldwide, mainly with the increasing of age [1]. Since the
42 population is gradually older, with the passage of time there will be an increase in the incidence of
43 POP of 46% between 2010 and 2050 [2]. Although they are not lethal diseases, these two pathologies
44 negatively influence the quality of life of women, including their social, sexual, physical and

45 psychological well-being [1,3]. The implantation of meshes to reinforce soft tissue defects and provide
46 an additional support to prolapsed organs and viscera is a common approach to treat POP and SUI
47 [4].

48 Vaginal meshes are commonly made of poly(propylene) (PP) or polyester, materials that already
49 used for hernia repair [5,6]. These materials are safe for hernia repair, but its safety was not properly
50 tested for pelvic floor applications [5]. However, they were approved by the US FDA [5,6]. Since
51 approval, multiple cases of complications associated to vaginal meshes have been reported [7]. The
52 main problem for these meshes is the different structure and motility of the pelvic floor when
53 compare with the abdominal wall. In addition to this, important movements and morphological
54 changes occur during a woman's life, and as a result, the material used to repair the pelvic floor must
55 be not only biocompatible, but also able to tolerate the stress and tension associated with such a
56 dynamic environment and at the same time flexible and elastic [5].

57 PP is the main polymer used for the production of synthetic meshes for POP surgery due to its
58 chemical stability and non-biodegradable property [8]. However, complications such as adhesion to
59 the viscera and high inflammatory response found in the repair of the pelvic floor [8] have led
60 researchers to study alternative solutions. Biodegradable/bioresorbable polymers, such as
61 poly(caprolactone) or poly(lactic acid) (PLA), have been used for mesh implant application with
62 mixed results [9–11]. In some cases, this type of implants can display mechanical failures due to their
63 degradation. For example, PLA₉₄ can present mechanical problems after 8 months [11]. Accordingly,
64 non-biodegradable polymers seem to be a safer approach. Recently, it was reported that
65 poly(urethane)-based meshes were safer and more suitable than PP for vaginal meshes production
66 [12,13]. Accordingly, polyurethane-based polymers seem to be the ideal candidate for this
67 application.

68 In addition to safer materials, new manufacturing methods can provide benefit to the resulting
69 medical devices. A potential technology to produce the aforementioned meshes is 3D printing. This
70 technology allows clinicians to prepare devices adapted to patient's anatomy and requirements [14–
71 17]. Furthermore, a wide range of materials can be used for 3D printing applications. These materials
72 include PLA, PP or nylon. PLA has been extensively used for biomedical applications and for 3D
73 printing applications [18–20]. PLA is one of the most widely used material for 3D printing
74 (specifically for fused deposition modelling) [20,21]. However, as described before, due to its
75 biodegradable nature is not the ideal candidate for vaginal mesh preparation. Interestingly,
76 poly(urethane), a promising material for pelvic floor surgery, has been used before for 3D printing
77 applications [14].

78 The flexibility of 3D printing also allows to combine polymeric materials with drugs to prepare
79 drug eluting devices [14,19,22]. This is extremely useful for implantable devices that have a relatively
80 high risk of infection [14,19,23]. If the device is loaded with antibiotics this will prevent bacterial
81 colonisation of its surface preventing infections [14,19]. There are a wide variety of techniques within
82 3D printing technology [16]. In the present work, fused deposition modelling (FDM) was used. This
83 technique relies on the extrusion of a polymeric filament through a hot nozzle to prepare objects. To
84 combine the polymers with drugs within the filament hot melt extrusion (HME) is needed. For this
85 purpose, a drug substance and the selected polymer are melted inside a rotating screw to mix them
86 and subsequently extrude them to form a filament [15]. This filament will be subsequently used for
87 FDM applications.

88 The aim of this work is to develop a new generation of vaginal mesh implants. For this purpose,
89 meshes will be prepared using thermoplastic poly(urethane) (TPU) and they will be loaded with an
90 antibacterial agent, levofloxacin (LFX) (drug commonly used to treat urinary infections), using fused
91 deposition modelling (FDM). This technique is the most common type of 3D printing. Three different
92 filaments of TPU containing 0.25%, 0.5%, and 1% of LFX were prepared through single hot-melt
93 extruder in order to be used for the 3D Printing FDM process. Mechanical strength, drug release and
94 antimicrobial properties were evaluated to confirm the efficiency of the meshes.

95
96

97 2. Materials and Methods

98 2.1. Materials

99 Elastollan® thermoplastic polyurethane (TPU) 80A pellets were used for this study and kindly
 100 provided by DISTRUPOL Ltd (A Univar Company, Co Dublin). Castor oil was purchased from Ransom,
 101 LFX ((S)-9-fluoro-2,3-dihydro-3-methyl-10-(4-methylpiperazin-1-yl)-7-oxo-7H-pyrido[1,2,3-de]-1,4-
 102 benzoxazine-6-carboxylic acid) >98% was obtained by Sigma Aldrich, and the phosphate buffered
 103 saline (PBS) tablets pH 7.4 from Merck. **The PP filament (2.85 mm diameter) was purchased from**
 104 **Verbatim (Japan).**

105 2.2. Preparation of TPU filaments containing LFX

106 In order to 3D print meshes, filaments were prepared using the Hot-Melt Extrusion (HME)
 107 technique by combining the TPU with LFX. An oil method was used to ensure a homogeneous
 108 distribution of the drug on the pellet's surface. TPU pellets (30 gr) were placed in 50 mL Falcon tubes
 109 and castor oil (30 µL) was added and vortexed for a few min in order for the pellets to be covered
 110 homogeneously by the oil. The pellets were transferred to a new 50 mL Falcon tubes to avoid drug
 111 wastage that could remain attached due to excess oil on the wall of the previous tubes, as previously
 112 reported [14]. Then, LFX was added in ratio of 0.25% w/w and the tube was vortexed in order to coat
 113 the pellets. Finally, the coated pellets were introduced in the filament extruder (3Devo, Utrecht, The
 114 Netherlands) using an extrusion speed range of 3-5 rpm and a filament diameter of 2.85 mm. The
 115 temperature was regulated directly during the extrusion over four heaters between 170°C and 200°C.
 116 The same procedure was performed for preparing filaments containing 0.5% and 1% of LFX. The
 117 filament formed using only TPU, which used for the preparation of blank meshes, was manufactured
 118 introducing directly the pellets into the extruder. **Formulations with their compositions to**
 119 **manufacture the filaments are presented in the Table 1.**

120 **Table 1.** Composition of TPU filaments containing LFX.

Formulations	TPU (g)	Castor oil (µL)	LFX (g)
TPU	30	-	-
0.25% LFX	30	30	0.075
0.50% LFX	30	30	0.15
1.00% LFX	30	30	0.3

121

122 2.3. Preparation of 3D printed meshes containing LFX

123 Meshes were printed with the drug-loaded and unloaded filaments that previously prepared
 124 with the extruder, using an Ultimaker 3 (Ultimaker B.V., Geldermalsen, The Netherlands) fused
 125 filament fabrication (FFF) system, furnished of two extruders with a 0.4 mm nozzle, and Cura®
 126 software. Different models were designed through a CAD-based software. **For the TPU meshes, the**
 127 **layer height was set at 0.1 mm with the in-fill setting on the software at 100%. The printing**
 128 **temperature was set at 190 °C and the printing speed was 12 mm/s. However, for the PP meshes, the**
 129 **printing temperature was set between 195 and 208 °C and the printing speed was 25 mm/s. These PP**
 130 **meshes were manufactured using the filament obtained from Verbatim.**

131 2.4. Characterization of 3D printed meshes

132 2.4.1. Mechanical properties

133 Meshes with 50 mm x 10 mm size were printed, and the fracture force was studied with
 134 TA.XTplus texture analyser (Stable Micro Systems, Surrey, UK). Each sample was vertically fixed
 135 with two clamps, with a distance between them of 40 mm, and stretched at a rate of 5 mm/s up to 200

136 mm. The experiment was repeated 4 times for each sample. The force/displacement curves were
137 recorded, and different parameters were obtained. The elastic limit of the resulting meshes were
138 obtained using the 0.2% offset method [24]. Additionally, the tensile stiffness was calculated from the
139 force/displacement curves as the slope of the initial linear region [25].

140 2.4.2 Fourier Transform Infrared (FT-IR) spectroscopy

141 The Fourier Transform Infrared (FT-IR) spectra of 1 cm x 1 cm meshes were recorded through a
142 Spectrum Two™ instrument (Perkin Elmer, Waltham, MA, USA). The spectra were recorded between
143 4000 cm⁻¹ and 600 cm⁻¹ applying a resolution of 4 cm⁻¹; total of 32 scans were collected.

144 2.4.3. Thermogravimetric analysis (TGA)

145 As the elastomer was subjected to high temperatures during the 3D-printing process, the
146 thermal degradation behaviour of the polymer was examined. Thermogravimetric analysis (TGA)
147 was performed to measure the weight loss of the TPU meshes containing LFX. For this purpose, a
148 small fragment of these meshes (3 mg and 10 mg) was used. TGA was performed using a Q500
149 Thermogravimetric analysis (TA instruments, Bellingham, WA, USA). Scans were run from room
150 temperature to 550 °C, at a speed rate of 10° C/min under a nitrogen flow rate of 50 ml/min

151 2.4.4. Scanning electron microscopy (SEM)

152 Scanning electron microscopy was used in order to investigate the surface morphologies of the
153 1 cm x 1 cm 3D-printed meshes containing 0.25, 0.5 and 1% of LFX compared with the blank mesh,
154 using samples before and after a 14-days release study. The meshes were examined using a Hitachi
155 TM3030 SEM (Tokyo, Japan), and images were taken with a magnification of 50x, 60x, 80x, 300x and
156 500x. Additionally, a Leica EZ4 D digital microscope (Leica, Wetzlar, Germany) was used to examine
157 the presence or not of drug aggregates within the extruded materials.

158 2.4.5. X-ray microcomputed tomography (μCT)

159 X-ray Microcomputed Tomography imaging was performed on 3D printed meshes using the
160 same approach previously reported [14]. Briefly, all the samples were analysed by using a Bruker
161 Skyscan 1275, with a Hamamatsu L11871 source (40kV, 250μA). The meshes were mounted vertically
162 on dental wax and positioned at 57.5 mm from the source, where camera to source distance was 286
163 mm. No filter was applied for an exposure time of 49ms. The images generated were 1536x1944 pixels
164 with a resolution of 17μm per pixel. A total of 1056 images were taken in 0.2° steps around one
165 hemisphere of the sample, with an average of 3 frames taken at each rotation step. Attenuation
166 thresholding was conducted manually, in order to eliminate speckle around the samples. The same
167 thresholding was applied within Bruker's CTan software, where the samples were further processed.

168 2.5. *In vitro* drug release studies

169 The release profile for the LFX was defined conducting release studies that allowed calculating
170 the amount of drug eluted from the LFX-loaded meshes. Each sample was placed in Eppendorf's
171 with 2 mL of PBS. Subsequently the Eppendorf's were located in a shaking incubator at 37°C at 40
172 rpm. After 1, 2, 4, 24, 48, 72, 96 and 120 hours the sample was removed from the tube, dried and
173 relocated in a new Eppendorf containing 2 mL of fresh PBS. Further studies performed also in new
174 samples for 7 and 14 days. The concentration of LFX was calculated after measuring the UV
175 absorbance of the solution taken from the Eppendorf's with a UV-visible plate reader (PowerWave
176 XS Microplate Spectrophotometer, Bio-Tek, Winooski, VT, USA) at a wavelength of 292 nm as
177 previously reported [26]. For each concentration (control, 0.25, 0.5 and 1%), 1 cm x 1 cm meshes were
178 used in series of 4.
179

180 2.6. In vitro microbiological analysis

181 Printed meshes (1 cm × 1 cm × 0.1 cm) were tested for inhibitory effect on bacterial cultures of
182 *Staphylococcus aureus* NCTC 10788 (Gram-positive) and *Escherichia coli* NSM59 (Gram-negative). *E.*
183 *coli* and *S. aureus* are examples of bacteria that can cause a variety of community- and hospital-
184 acquired infections. This in vitro microbiological analysis was performed according to a previous
185 published work, with some modifications [14]. Briefly, bacteria were grown overnight at 37 °C in
186 Mueller-Hinton (MH) broth. For each bacterium, 50 µL of the overnight culture were added to 5 mL
187 of MH soft agar. This mixture was vortexed and then poured on top of the MH agar plate. Finally,
188 meshes were placed in the centre of the plate and incubated for 24 h at 37 °C. The inhibition zone
189 caused for both bacterial strains was then measured in mm. Moreover, inoculated plates for each
190 bacterial strain were also incubated as a positive control. The results were expressed as mean ±
191 standard deviation of 5 replicates.

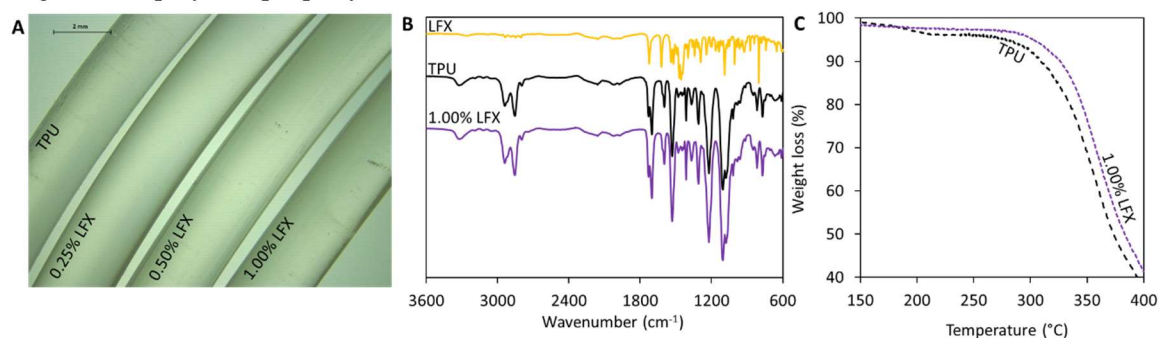
192 2.7. Statistical Analysis

193 Quantitative data were expressed as a mean ± standard deviation, $n \geq 3$. The statistical analysis
194 was performed using a one-way analysis of variance (ANOVA), $p < 0.05$ was considered to be
195 statistically significant.

196 3. Results

197 3.1. Preparation and characterisation of TPU filaments and meshes containing LFX

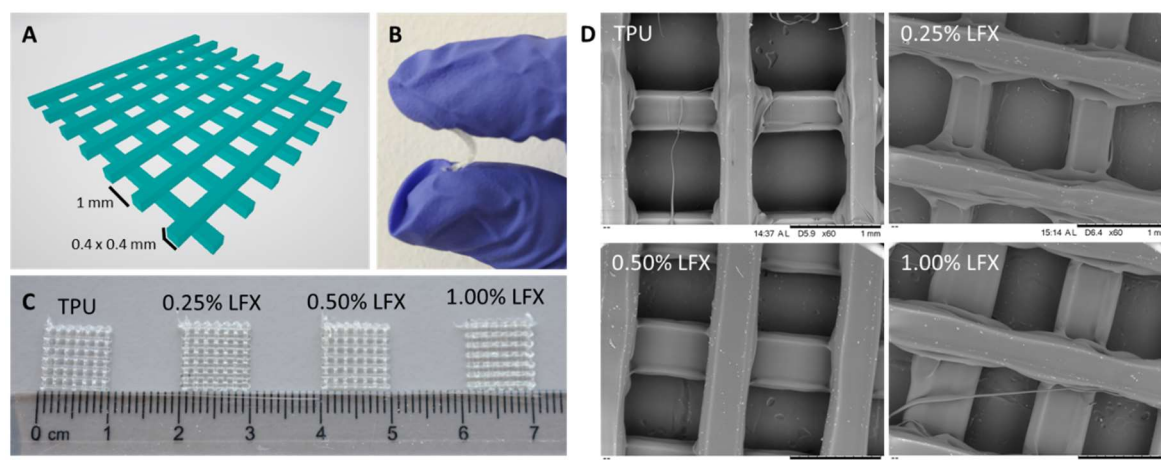
198 The extrusion of the TPU pellets containing the different LFX concentrations were used to
199 produce smooth and flexible filaments of 2.85 mm in diameter (Figure 1A). The resulting materials
200 contained different amounts of LFX ranging from 0.25 to 1% (w/w). All the filaments prepared using
201 hot-melt extrusion showed the same translucent colour. No visible aggregates of drug were seen
202 within the extruded materials. Considering that LFX is a white solid this suggests that the antibiotic
203 was mixed with the molten TPU within the extrusion process. Moreover, the results suggest that TPU
204 and LFX can be mixed properly using a single screw extruder following the pellet coating method.
205 Otherwise, a more complicated equipment such as a twin-screw extruder will be required to mix the
206 drug and the polymer properly.



207
208 **Figure 1.** Microscopy image of the TPU and LFX loaded TPU filaments (A). FTIR spectra of LFX, TPU and TPU
209 containing 1% of LFX (B). TGA of TPU and TPU containing 1% LFX (C).
210

211 FT-IR and TGA were used to try to establish if there were any interaction between TPU and LFX.
212 The FT-IR spectra of the materials containing LFX showed the same peaks that the blank TPU (Figure
213 1B). The drug loadings selected for the present work was too low to be able to produce any changes
214 in FT-IR spectra. However, TGA measurements (Figure 1C) shows that when LFX was combined
215 with TPU using hot melt extrusion the resulting material presented different thermal degradation
216 behaviour. Filaments containing LFX started to degrade at higher temperatures than blank TPU
217 filaments. In order to compare both materials, the onset temperatures (T_{onset}) were measured. T_{onset}
218 denotes the temperature at which the weight loss begins (5% weight loss). The onset temperature for
219 TPU was 280 °C while the recorded onset temperature for TPU containing 1% of LFX was 303 °C. As

220 mentioned before this temperature differences can be attributed to interactions between the TPU and
 221 the LFX.
 222

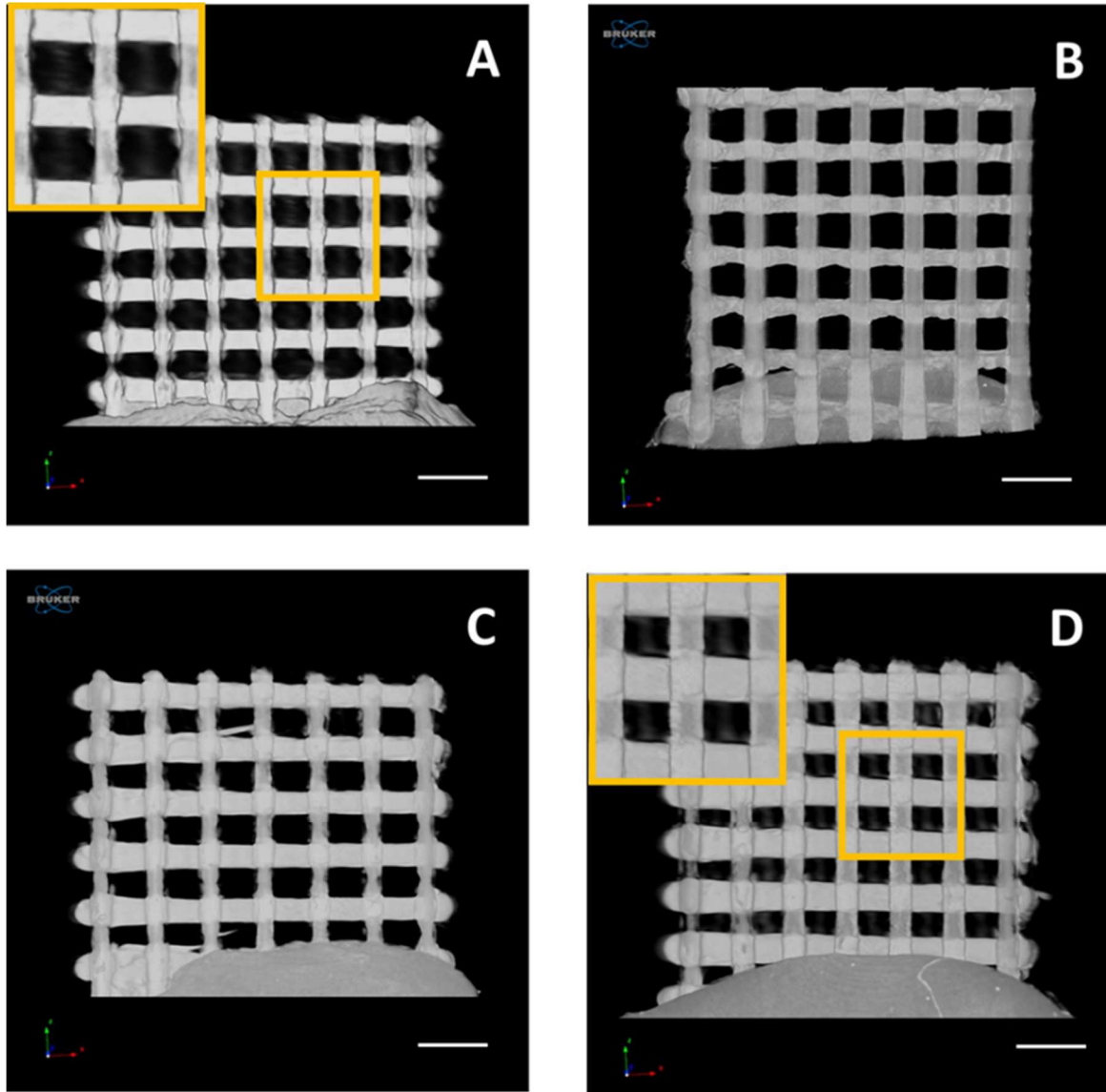


223 **Figure 2.** CAD 3D image of the two layer meshes with its dimensions (A). Representative image showing the
 224 flexibility of a TPU-based mesh (B). Image of TPU and TPU loaded with LFX 3D printed meshes (C). SEM images
 225 of TPU and LFX loaded TPU 3D printed meshes (D).
 226
 227

228 The TPU filaments previously described were used to prepare different types of surgical meshes.
 229 These designs were prepared using Computer Aided Software and subsequently prepared using
 230 fused deposition modelling. Figure 2A shows the designs used to prepare the meshes with their
 231 dimensions. Moreover, Figure 2C shows some 1x1 cm mesh prototypes produced using the filaments
 232 described in section 3.1. As expected, all these prototypes presented the same appearance as LFX was
 233 completely mixed with the TPU. These resulting meshes are flexible as can be seen in Figure 2B. These
 234 results can be corroborated by using SEM (Figure 2D). The microscopy images showed that all the
 235 resulting meshes showed the same structure and no signs of drug aggregation within the surface of
 236 the devices.

237 The 3D printed samples were analysed by using a Bruker Skyscan 1172 system (Figure 3), in
 238 order to investigate samples' topology as well as drug distribution within their architecture. As it
 239 could be seen in Figure 3B-D, the incorporation of LFX did not affect the 3D printed mesh
 240 morphology, which resulted very similar for all the analysed samples and comparable to the one of
 241 pure TPU80 (Figure 3A).

242 In addition, as shown in the representative reconstruction images, the meshes exhibited the same
 243 topology. Particularly, even at the highest concentration of LFX (Figure 3D), no traces of particles
 244 were detected within the printed meshes, thus indicating a uniform distribution of the drug,
 245 regardless the concentration tested. Moreover, according to this outcome it was further demonstrated
 246 the effectiveness of the manufacturing process from drug incorporation to 3D printed sample
 247 fabrication.
 248

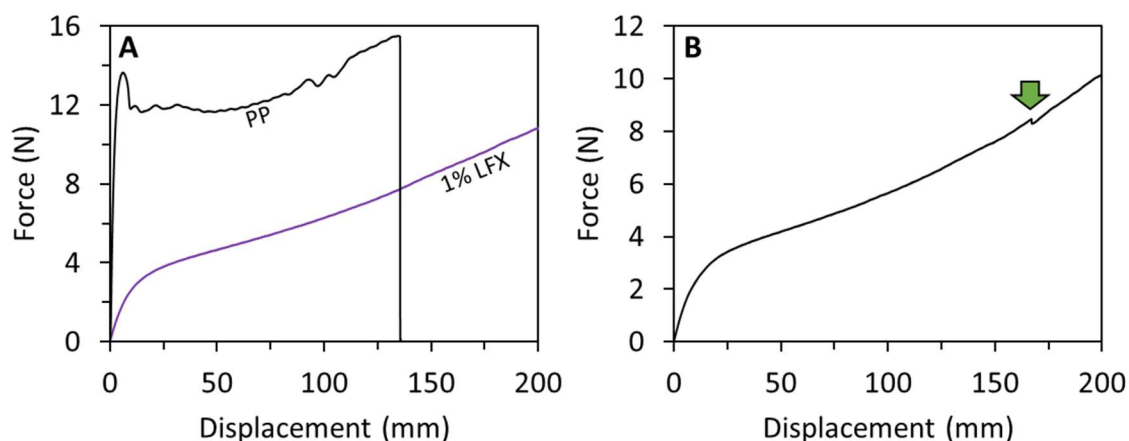


249
 250 **Figure 3.** μ CT reconstructions in the xz plane of pure TPU80 mesh (A) and TPU80 mesh loaded with 0.25% (B),
 251 0.5% (C) and 1% (D) of LFX [scale bar = 2 mm].

252 3.2. Mechanical Characterisation of LFX 3D printed meshes

253 The mechanical properties of two-layered mesh implants prepared using fused deposition
 254 modelling were measured. Figure 4 shows representative force/displacement graphs for the prepared
 255 meshes. All the TPU-based meshes showed similar profiles. The first region of the graph showed
 256 elastic behaviour (initial linear section of the graph) and then when higher forces are applied the
 257 meshes showed plastic deformation (see Figures 4A and 4B). It is important to note that they did not
 258 fully break under the testing conditions (200 mm of elongation) in some cases they show some minor
 259 fractures during the last stages of the test (Figure 4B). However, this does not happen consistently in
 260 all the meshes. This was observed only in two cases. It is important to note that these partial fractures
 261 happened after the mesh elongated more than 3 times its original size. On the other hand, meshes
 262 made of PP were prepared to compare the obtained results with the material typically used for mesh
 263 implant manufacturing. PP showed a different mechanical behaviour than TPU-based meshes. PP
 264 meshes failed during the test as they showed a clear and reproducible fracture point (Figure 4A).

265



266
267 **Figure 4.** Force/displacement graphs obtained for TPU meshes containing 1% LFX and PP meshes (A).
268 Force/displacement graph showing a small fracture for a TPU-based mesh (B). The arrow indicates the fracture
269 point.

270 The elastic limit and the tensile stiffness were evaluated from the force/displacement curves. The
271 elastic limit was measured from the force/displacement curves using the 0.2% offset method. This
272 value represents the force required to produce a 0.2% of plastic deformation of the meshes. All TPU-
273 based meshes showed elastic limits around 1 N (Table 2). Moreover, statistical analysis showed that
274 there were no significant differences between all these values ($p > 0.05$). These results suggest that
275 LFX loadings of up to 1% (w/w) did not alter the mechanical properties of TPU. This is important for
276 the applications as TPU was selected due to its elasticity as opposed to conventional PP meshes.
277 Polypropylene meshes showed significantly higher elastic limit than the TPU-based meshes ($p < 0.05$).
278 This is consistent with the nature of the material that is not an elastic material as opposed to TPU.
279 Finally, the tensile stiffness of the mesh implants was evaluated. Again, the results showed that all
280 TPU-based meshes showed equivalent values of tensile stiffness ca. 0.4 N/mm ($p > 0.05$). Moreover,
281 PP meshes showed significantly higher values of tensile stiffness ($p < 0.05$). These values showed that
282 PP required higher forces to elongate within the elastic region of the material. Accordingly, PP is a
283 tougher material with lower elasticity. Again, TPU seems a more suitable approach for mesh implant
284 manufacture due to its elasticity.

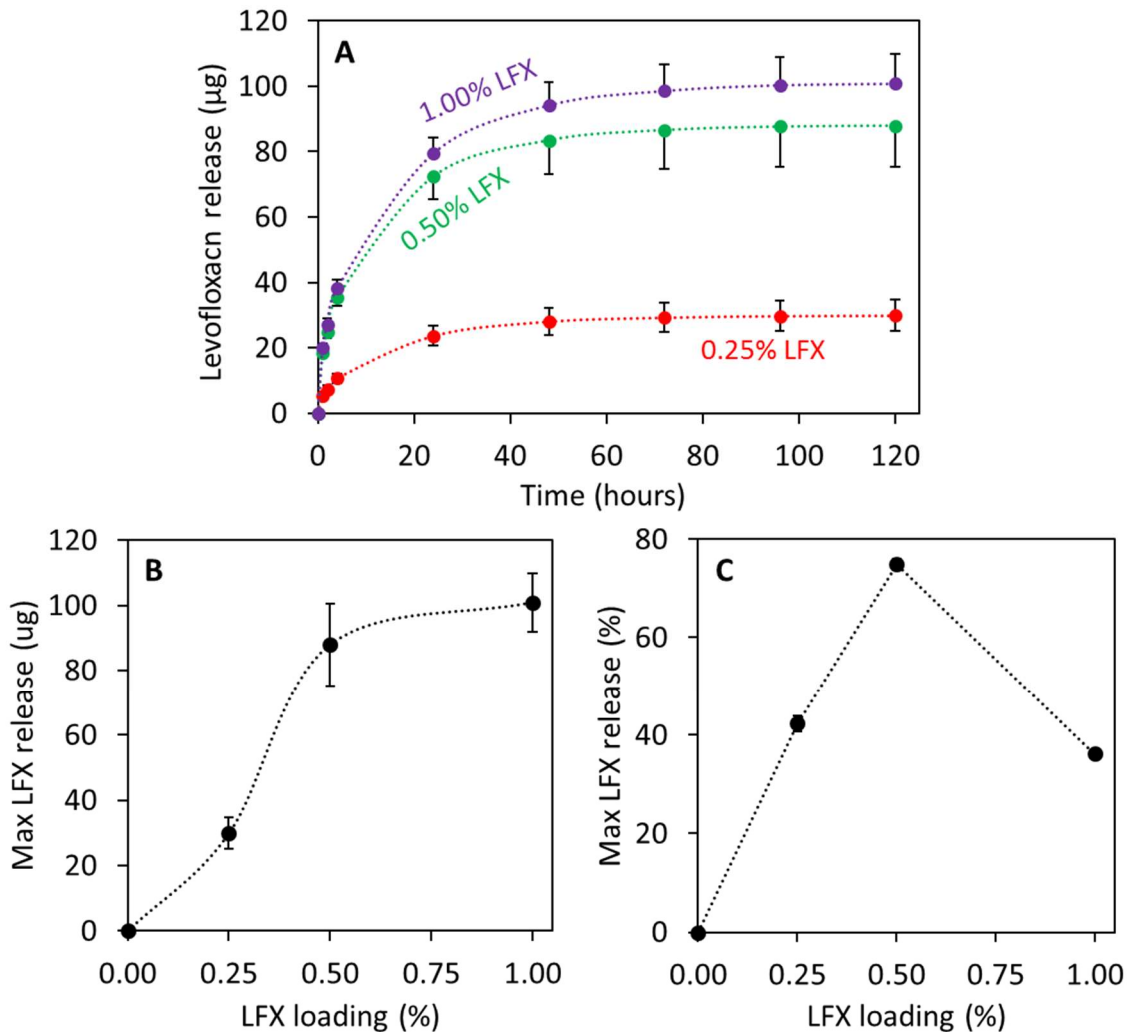
285 **Table 2.** Mechanical properties obtained for the 3D printed meshes formed by two layers.

	LFX Content (%)	Elastic Limit (N)	Tensile Stiffness (N/mm)	Fracture Force (N)	Elongation at break (mm)
TPU	0.00	1.2 ± 0.4	0.44 ± 0.12	-	-
LFX 0.25%	0.25	1.0 ± 0.2	0.32 ± 0.06	-	-
LFX 0.50%	0.50	1.1 ± 0.1	0.37 ± 0.04	-	-
LFX 1.00%	1.00	1.3 ± 0.2	0.45 ± 0.08	-	-
PP	0.00	6.5 ± 0.2	6.05 ± 0.83	15.42 ± 0.66	129 ± 7

286 3.3. LFX release from 3D printed meshes

287 Figure 5 shows the LFX release from 3D printed meshes. Figure 5A shows the LFX released as a
288 function of time for the 3D printed meshes. The prepared meshes are capable of providing sustained
289 release of LFX for at least 3 days. Additionally, it can be seen that all the release profiles showed the
290 similar shapes. The total amount of LFX released after 5 days (Figure 5B) increased with drug loading.
291 However, there is a significant increase in the drug loading when the LFX loading increased from
292 0.25% to 0.5% ($p > 0.05$). When drug loading increased from 0.5% to 1% a small increment in drug
293 release was observed. However, statistical analysis revealed that this difference is not statistically
294 significant ($p < 0.05$). Accordingly, it can be hypothesised that LFX could be interacting with TPU

295 within the meshes and this prevent higher drug release. This is consistent with the results described
 296 in section 3.1. These results are more obvious when the release was expressed as percentage of the
 297 initial drug loading (Figure 5C). This graph showed some interesting results. The percentage of drug
 298 release increase with drug loading up to a maximum. This maximum was obtained for meshes
 299 containing 0.5% of LFX. Subsequently, the percentage of drug release decreases when drug loading
 300 was increased up to 1% ($p < 0.05$). This showed that LFX/TPU interactions are taking place and
 301 reducing drug release.



302

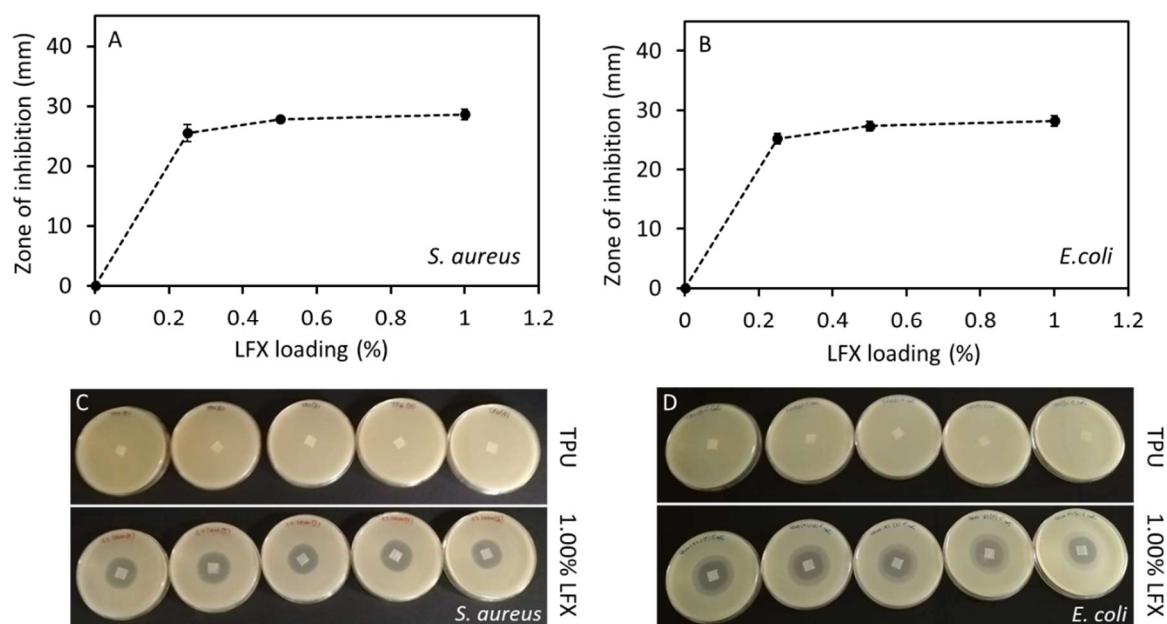
303 **Figure 5.** LFX release as a function of time for different LFX loaded 3D printed meshes (A). Maximum LFX
 304 release expressed in µg (B) and percentage (C) as a function of initial LFX drug loading.

305 3.4. Antimicrobial properties of LFX loaded 3D printed meshes

306 Printed meshes (1 cm × 1 cm × 0.1 cm) containing different LFX concentrations were tested for
 307 antimicrobial effect on a bacterial culture of *S. aureus* and *E. coli* in order to evaluate good examples
 308 of bacteria that are involved in a variety of community-and hospital-acquired infections. The results
 309 of the zone of inhibition are presented in the Figure 6. In this case, the zone of inhibition indicates
 310 that both used bacteria either at the surface of the meshes or even for an area extending outwards
 311 from the mesh's surface is inhibited. All the meshes containing LFX showed a clear zone of inhibition
 312 in both *S. aureus* and *E. coli* plates. As expected, the results showed no zone of inhibition in plates
 313 containing the control meshes without LFX.

314 The zones of inhibition in both *S. aureus* and *E. coli* plates were increased by increasing the
 315 amount of LFX. The diameter of the zone of inhibition in the *S. aureus* plates with TPU meshes

316 containing LFX ranged from 25.5 ± 1.4 mm to 28.6 ± 0.8 mm, and from 25.2 ± 0.9 to 28.2 ± 0.8 in the *E.*
 317 *coli* plates. Statistical analysis showed that there were significant differences between the zones of
 318 inhibition caused by meshes containing 0.25% and 0.5% or 1% LFX ($p < 0.05$). This behaviour was
 319 observed for both cultures, *S. aureus* and *E. coli*. However, there were no significant differences in the
 320 zone of inhibition caused by meshes containing 0.5% and 1% LFX ($p > 0.05$). Once again, this trend
 321 was observed for both bacterial strains. These results are in line with the obtained drug release
 322 profile for the meshes containing LFX (Figure 5A). In addition, when the zones of inhibition of *E. coli*
 323 and *S. aureus* were compared for the same concentration of LFX (0.25%, 0.5% and 1%), no significant
 324 differences were observed for any LFX concentration ($p > 0.05$). Therefore, it can be inferred that LFX
 325 had the same impact on both bacterial strains, which are the most frequent causes of many common
 326 bacterial infections.



327 **Figure 6.** Correlation between the diameter of the zone of inhibition of *S. aureus* (A) and *E. coli* (B) and the
 328 concentration of LFX. Agar plates showing the zone of inhibition of meshes without LFX (TPU) and containing
 329 1% of LFX for both bacterial strains, *S. aureus* (C) and *E. coli* (D).

330 4. Discussion

331 Historically, PP has been the choice material for pelvic floor repair since 1995 [13]. However, it
 332 has been shown that this material is not the ideal candidate for these applications due to the
 333 mechanical mismatch between the elastic paravaginal tissue and the strong and rigid PP [27].
 334 Accordingly, the mechanical properties of PP mesh have generated multiple problems after mesh
 335 implantation. According to the US FDA the use of PP mesh for pelvic floor repair can lead to serious
 336 complications associated with tissue erosion [28,29]. The ideal material for the production of pelvic
 337 floor repair mesh implants should possess elasticity and strength [12].

338 The present work describes the use of fused deposition modelling for the production of mesh
 339 implants for potential pelvic organ reconstructive surgery. TPU was selected as the ideal candidate
 340 for this purpose due to its elasticity and previously demonstrated biocompatibility [12,13,18]. This
 341 material has been used before for mesh implant manufacturing showing superior capabilities than
 342 PP implants [12,13]. Additionally, TPU was combined with an antibiotic drug to prevent infection of
 343 this implantable material after surgery. Mesh-related infections are not common but when they occur
 344 they can compromise patients' well-being even leading to excision of the mesh implant or sepsis [30].

345 LFX was the antibiotic chosen for this application. In a previous work it was loaded in meshes
 346 prepared using electrospinning for hernia repair [26]. This antibiotic was combined with TPU using
 347 hot-melt extrusion to prepare filaments for further FDM applications. The materials showed
 348 homogeneous distribution of the drug. This was achieved using a single screw extruder coating the

349 TPU pellets with LFX. This method has been previously used with successful results [14,19,31,32].
350 This is a quick way to obtain good mixtures between the drug and the polymer using a single screw
351 extruder that is more accessible than a complicated and expensive twin-screw extruder. Figure 1A
352 shows that the drug was properly dispersed within the material. FTIR results did not show any
353 noticeable peak shift (Figure 1B). As mentioned before this can be due to the low drug loading. Similar
354 behaviour was reported before for the combination of TPU and tetracycline or poly(urethane) and
355 ciprofloxacin, a drug similar to LFX [14,33]. On the other hand, TGA results (Figure 1C) shows that
356 there was interaction between LFX and TPU. Similar behaviour was reported when TPU was
357 combined with tetracycline, ciprofloxacin or Schiff base additives [14,33,34]. It has been proposed
358 that the C=O groups present in the TPU urethane groups can establish non-covalent interactions with
359 the drug.

360 The interaction of LFX with TPU can explain the behaviour obtained in the drug release profiles.
361 In these experiments, meshes containing 1% of LFX showed a lower percentage of LFX released from
362 the meshes than meshes containing 0.5% of LFX. The interactions between the polymer and the drug
363 prevents a higher drug release. This has been observed previously for other drugs such as
364 dipyridamole loaded into polyurethane [35]. Similarly, lower drug loadings (0.25% LFX) showed low
365 release too. TPU is a non-degradable/hydrophobic polymer and, accordingly, the drug cargo located
366 inside the material will not be released. Finally, the TPU meshes described in the present work are
367 capable of providing releases of LFX for at least 3 days. A previously published work describing the
368 use of electrospinning to prepare poly(caprolactone) surgical meshes loaded with LFX (0.5%) showed
369 that this system was capable of providing drug release over 1 day. However, the nature of the mesh
370 forming polymer was completely different.

371 This work was not only focused on the development of safer materials for mesh implant
372 manufacturing but the use of techniques that allow clinicians to customize the mesh to patient's needs
373 in a simple way. Therefore, FDM seems like an ideal technique for this purpose. TPU based meshes
374 were successfully prepared using FDM (Figure 2). As expected, all the meshes had the same
375 appearance and now noticeable drug aggregation was observed (Figure 2). Computed tomography
376 was used to confirm drug distribution within the mesh matrix. Again, the results suggested that the
377 drug was uniformly distributed within the mesh. In a previous study computed tomography
378 suggested that the combination of similar TPU with tetracycline showed some drug accumulation in
379 certain parts of the material [14]. In this case, tetracycline was distributed all over the material, but
380 some accumulation was observed using computed tomography.

381 The observed mechanical properties of the resulting meshes proved the initial approach: the
382 resulting materials showed elastic behaviour unlike PP. TPU-based meshes showed stiffness values
383 ca. 0.4 N/mm while commercial PP meshes showed values ranging between 2 and 6 N/mm [25]. The
384 design of the commercial meshes is different than the one proposed in the present paper but the
385 testing conditions for these commercial meshes were similar. Some comparisons can be made. In
386 order to compare the effect of the material in the mechanical properties, PP meshes were prepared
387 using the same design used for the TPU based materials. Obviously, this PP is not exactly the same
388 than the one used in conventional meshes but it is a good example to compare the behaviour of both
389 materials. The stiffness results obtained for PP (ca. 6 N/mm) was higher than the one obtained for
390 TPU meshes and the Force/displacement profile was completely different. Moreover, the stiffness
391 values obtained for PP meshes were slightly higher than the previously reported results for
392 commercial PP meshes (up to 5.3715 N/mm) [25]. However, the PP meshes tested in this work showed
393 a different design than the commercial meshes. The mechanical characteristics of the material are
394 important as it has been reported that materials with higher flexibility seem to adhere and conform
395 to the tissues better than more rigid/stiffer meshes [36]. The design and size of the meshes can be
396 hanged easily due to the versatility of FDM.

397 The 3D-printed meshes had a bacteriostatic activity on both *S. aureus* and *E. coli* cultures (Figure
398 6). This fact supports the premise that the extrusion and 3D printing processes did not affect the
399 bacteriostatic activity of LFX. The risk of toxicity of these coated medical devices could be an
400 important issue. Therefore, the possibility to print these medical devices using a small amount of the

401 desired drug, and still have bacteriostatic activity, clearly minimizes the risk of toxicity in the patients.
402 For instance, medical devices such as thermoplastic polyurethane (TPU) catheters were 3D-printed
403 using up to 1% of tetracycline [14], thereby minimizing the risk of infection. Also, Weisman et al. [31]
404 in a different study, reported the possibility to print poly(lactic acid) (PLA) catheters using up to 2.5%
405 of gentamicin. Additionally, is also possible to print medical devices using higher percentage of
406 drugs. Thus, for example, Genina et al. [37] 3D-printed drug-loaded intrauterine devices using
407 different grades of ethylene vinyl acetate containing 5% and 15% of indomethacin.

408 PLA pellets coated with 1 wt% gentamicin were used to fabricate mesh prototypes for hernia
409 repair [38]. In this study, they obtained a zone of inhibition of 1.1 ± 0.1 cm² for *E. coli* and 1.2 ± 0.1 cm²
410 for *S. aureus*. In a different work, polyvinyl alcohol (PVA) 3D meshes loaded with iodine were
411 manufactured and these also showed a zone of inhibition against *E. coli* and *S. aureus* [39]. These
412 results were far below to those found in our work. The diameter of the zone of inhibition in the *S.*
413 *aureus* plates with TPU meshes of 0.25% LFX was 25.5 ± 1.4 mm and 28.6 ± 0.8 mm for meshes
414 containing 1% LFX. As mentioned above, there were no significance differences between these results
415 and the ones obtained in the *E. coli* plates ($p > 0.05$). Therefore, it can be inferred that even the lower
416 concentration (0.25%) of LFX had a significant zone of inhibition on both bacterial stains, which
417 further minimises the risk of toxicity.

418 The use of medical devices such as transvaginal meshes, catheters or ventilators could be
419 associated with the development of “nosocomial” or “health-care associated infections” (HCAIs)
420 [40,41]. Although bacteria, viruses or fungal parasites can cause these infections, bacteria are the most
421 common pathogens responsible for HCAI. Among these, bacterial species as *S. aureus* and *E. coli* have
422 a major impact [42]. *S. aureus* is one of the most important pathogens responsible for nosocomial
423 infections [43]. Moreover, *E. coli* is an emerging nosocomial pathogen, which is the leading cause of
424 urinary tract infections (UTI) while, *S. aureus* is rarely found in these infections [43,44]. These
425 infections may result in prolonged stays in the different health-care facilities, such as hospitals while
426 increasing health-care costs [45]. Hence, the use of these 3D-printed meshes could decrease the rate
427 of bacterial infections caused by the implant.

428 The majority of the FDM applications describing the combination of polymers with drugs are
429 focused on the development of oral solid dosage forms [46,47]. We believe that this technology has
430 potential to be used for the manufacturing of medicated devices that can be produced on demand for
431 a patient before a specific treatment/surgery. Previously we reported the use of FDM for dialysis
432 catheter manufacturing [14,19] or antioxidant wound dressings. Some preliminary work has been
433 done about the use of 3D printing for mesh implant manufacture. However, these works were not
434 realistic as they propose the use of materials such as PLA or PCL that are biodegradable and do not
435 present appropriate mechanical properties for this task [38,48,49]. Some of these works incorporated
436 some antibiotics to the material. However, these works were not realistic due to material selection,
437 but these studies worked as a proof of concept showing the potential of 3D printing for this purpose.
438 Additionally, some recent work described the potential of using FDM as a tool for mesh implant
439 manufacturing using PP [50]. The limitations of this material have been described previously.
440 Moreover, these authors incorporated ciprofloxacin into the meshes by dip coating the implants. This
441 is not ideal as the manufacturing involves a two-step process. In the present work, the mesh is
442 produced directly containing the drug within the device.

443 Further research needs to be conducted about the *in vivo* biocompatibility of the meshes and
444 shape optimization to adapt the mechanical properties of the mesh to patient’s needs. The present
445 work is a proof of concept that shows the potential of FDM technology to prepare elastic anti-infective
446 materials. Finally, there are still regulatory aspects that should be addressed before 3D printing can
447 be approved as a manufacturing technology for surgical devices. The US FDA has published some
448 guidelines to manufactures about the appropriate use of this technology [51].

449 **Author Contributions:** Conceptualization, E.L. and D.A.L.; methodology, J.D.-R., C.M., E.M., I.G.-R., B.F.G. and
450 E.L.; investigation and formal analysis, J.D.-R., C.M., E.L. and E.M.; data curation, J.D.-R., C.M. and E.L.; writing,
451 J.D.-R., C.M., E.L. and D.A.L.; writing—review and editing, J.D.-R., C.M., E.M., I.G.-R., B.F.G., L.C., E.L. and
452 D.A.L.; and supervision, E.L. and D.A.L.

453 **Funding:** This research received no external funding.

454 **Conflicts of Interest:** The authors declare no conflict of interest.

455 **References**

- 456 1. Wu, Y. (Maria); Welk, B. Revisiting current treatment options for stress urinary incontinence and pelvic
457 organ prolapse: a contemporary literature review. *Res. Reports Urol.* **2019**, *Volume 11*, 179–188.
- 458 2. Mangir, N.; Chapple, C.R.; MacNeil, S. Synthetic Materials Used in the Surgical Treatment of Pelvic
459 Organ Prolapse: Problems of Currently Used Material and Designing the Ideal Material. In *Pelvic Floor*
460 *Disorders*; Rizvi, R., Ed.; InTech, 2018; Vol. i, p. 13 ISBN 978-1-78923-245-5.
- 461 3. Vergeldt, T.F.M.; Weemhoff, M.; IntHout, J.; Kluivers, K.B. Risk factors for pelvic organ prolapse and its
462 recurrence: a systematic review. *Int. Urogynecol. J.* **2015**, *26*, 1559–1573.
- 463 4. Niaounakis, M. Medical, Dental, and Pharmaceutical Applications. In *Biopolymers: Applications and*
464 *Trends*; Niaounakis, M., Ed.; Elsevier, 2015; pp. 291–405 ISBN 978-0-323-35399-1.
- 465 5. Mironska, E.; Chapple, C.; MacNeil, S. Recent advances in pelvic floor repair. *F1000Research* **2019**, *8*, 778.
- 466 6. Rac, G.; Younger, A.; Clemens, J.Q.; Kobashi, K.; Khan, A.; Nitti, V.; Jacobs, I.; Lemack, G.E.; Brown, E.T.;
467 Dmochowski, R.; et al. Stress urinary incontinence surgery trends in academic female pelvic medicine
468 and reconstructive surgery urology practice in the setting of the food and drug administration public
469 health notifications. *Neurourol. Urodyn.* **2017**, *36*, 1155–1160.
- 470 7. *Obstetrical and Gynecological Devices; Reclassification of Surgical Mesh for Transvaginal Pelvic Organ Prolapse*
471 *Repair*; 2016; Vol. 81;.
- 472 8. Mancuso, E.; Downey, C.; Doxford-Hook, E.; Bryant, M.G.; Culmer, P. The use of polymeric meshes for
473 pelvic organ prolapse: Current concepts, challenges, and future perspectives. *J. Biomed. Mater. Res. Part*
474 *B Appl. Biomater.* **2019**, jbm.b.34432.
- 475 9. FitzGerald, J.; Kumar, A. Biologic versus Synthetic Mesh Reinforcement: What are the Pros and Cons?
476 *Clin. Colon Rectal Surg.* **2014**, *27*, 140–148.
- 477 10. Hympanová, L.; Rynkevic, R.; Román, S.; Mori da Cunha, M.G.M.C.; Mazza, E.; Zündel, M.; Urbánková,
478 I.; Gallego, M.R.; Vange, J.; Callewaert, G.; et al. Assessment of Electrospun and Ultra-lightweight
479 Polypropylene Meshes in the Sheep Model for Vaginal Surgery. *Eur. Urol. Focus* **2018**.
- 480 11. De Tayrac, R.; Chentouf, S.; Garreau, H.; Braud, C.; Guiraud, I.; Boudeville, P.; Vert, M. In vitro
481 degradation and in vivo biocompatibility of poly(lactic acid) mesh for soft tissue reinforcement in
482 vaginal surgery. *J. Biomed. Mater. Res. - Part B Appl. Biomater.* **2008**, *85*, 529–536.
- 483 12. Shafaat, S.; Mangir, N.; Regureos, S.R.; Chapple, C.R.; MacNeil, S. Demonstration of improved tissue
484 integration and angiogenesis with an elastic, estradiol releasing polyurethane material designed for use
485 in pelvic floor repair. *Neurourol. Urodyn.* **2018**, *37*, 716–725.
- 486 13. Hillary, C.J.; Roman, S.; Bullock, A.J.; Green, N.H.; Chapple, C.R.; MacNeil, S. Developing Repair
487 Materials for Stress Urinary Incontinence to Withstand Dynamic Distension. *PLoS One* **2016**, *11*,
488 e0149971.
- 489 14. Mathew, E.; Domínguez-Robles, J.; Stewart, S.; Mancuso, E.; O'Donnell, K.; Larraneta, E.; Lamprou, D.A.
490 Fused Deposition Modelling as an Effective Tool for Anti-Infective Dialysis Catheter Fabrication. *ACS*
491 *Biomater. Sci. Eng.* **2019**, acsbiomaterials.9b01185.
- 492 15. Mathew, E.; Domínguez-Robles, J.; Larrañeta, E.; Lamprou, D.A. Fused Deposition Modelling as a
493 Potential Tool for Antimicrobial Dialysis Catheters Manufacturing: New Trends vs. Conventional
494 Approaches. *Coatings* **2019**, *9*, 515.
- 495 16. Liang, K.; Brambilla, D.; Leroux, J.-C. Is 3D Printing of Pharmaceuticals a Disruptor or Enabler? *Adv.*

- 496 *Mater.* **2019**, *31*, 1805680.
- 497 17. Trenfield, S.J.; Awad, A.; Madla, C.M.; Hatton, G.B.; Firth, J.; Goyanes, A.; Gaisford, S.; Basit, A.W.
- 498 Shaping the future: recent advances of 3D printing in drug delivery and healthcare. *Expert Opin. Drug*
- 499 *Deliv.* **2019**, *16*, 1081–1094.
- 500 18. Stewart, S.; Domínguez-Robles, J.; Donnelly, R.; Larrañeta, E. Implantable Polymeric Drug Delivery
- 501 Devices: Classification, Manufacture, Materials, and Clinical Applications. *Polymers (Basel)*. **2018**, *10*,
- 502 1379.
- 503 19. Domínguez-Robles, J.; Martin, N.; Fong, M.; Stewart, S.; Irwin, N.; Rial-Hermida, M.; Donnelly, R.;
- 504 Larrañeta, E. Antioxidant PLA Composites Containing Lignin for 3D Printing Applications: A Potential
- 505 Material for Healthcare Applications. *Pharmaceutics* **2019**, *11*, 165.
- 506 20. N. Turner, B.; Strong, R.; A. Gold, S. A review of melt extrusion additive manufacturing processes: I.
- 507 Process design and modeling. *Rapid Prototyp. J.* **2014**, *20*, 192–204.
- 508 21. Matos, B.D.M.; Rocha, V.; da Silva, E.J.; Moro, F.H.; Bottene, A.C.; Ribeiro, C.A.; dos Santos Dias, D.;
- 509 Antonio, S.G.; do Amaral, A.C.; Cruz, S.A.; et al. Evaluation of commercially available polylactic acid
- 510 (PLA) filaments for 3D printing applications. *J. Therm. Anal. Calorim.* **2019**, *137*, 555–562.
- 511 22. Domínguez-Robles, J.; Larrañeta, E.; Fong, M.L.; Martin, N.K.; Irwin, N.J.; Mutjé, P.; Tarrés, Q.; Delgado-
- 512 Aguilar, M. Lignin/poly(butylene succinate) composites with antioxidant and antibacterial properties
- 513 for potential biomedical applications. *Int. J. Biol. Macromol.* **2020**, *145*, 92–99.
- 514 23. Muwaffak, Z.; Goyanes, A.; Clark, V.; Basit, A.W.; Hilton, S.T.; Gaisford, S. Patient-specific 3D scanned
- 515 and 3D printed antimicrobial polycaprolactone wound dressings. *Int. J. Pharm.* **2017**, *527*, 161–170.
- 516 24. Hou, X.; Zheng, W.; Kodur, V.; Sun, H. Effect of temperature on mechanical properties of prestressing
- 517 bars. *Constr. Build. Mater.* **2014**, *61*, 24–32.
- 518 25. Afonso, J.S.; Martins, P.A.L.S.; Girao, M.J.B.C.; Natal Jorge, R.M.; Ferreira, A.J.M.; Mascarenhas, T.;
- 519 Fernandes, A.A.; Bernardes, J.; Baracat, E.C.; Rodrigues de Lima, G.; et al. Mechanical properties of
- 520 polypropylene mesh used in pelvic floor repair. *Int. Urogynecol. J.* **2008**, *19*, 375–380.
- 521 26. Hall Barrientos, I.J.; Paladino, E.; Brozio, S.; Passarelli, M.K.; Moug, S.; Black, R.A.; Wilson, C.G.;
- 522 Lamprou, D.A. Fabrication and characterisation of drug-loaded electrospun polymeric nanofibers for
- 523 controlled release in hernia repair. *Int. J. Pharm.* **2017**, *517*, 329–337.
- 524 27. Li, X.; Kruger, J.A.; Jor, J.W.Y.; Wong, V.; Dietz, H.P.; Nash, M.P.; Nielsen, P.M.F. Characterizing the ex
- 525 vivo mechanical properties of synthetic polypropylene surgical mesh. *J. Mech. Behav. Biomed. Mater.* **2014**,
- 526 *37*, 48–55.
- 527 28. Bako, A.; Dhar, R. Review of synthetic mesh-related complications in pelvic floor reconstructive surgery.
- 528 *Int. Urogynecol. J.* **2009**, *20*, 103–111.
- 529 29. *Urogynecologic Surgical Mesh: Update on the Safety and Effectiveness of Transvaginal Placement for Pelvic*
- 530 *Organ Prolapse*; 2011;
- 531 30. Mangir, N.; Roman, S.; Chapple, C.R.; MacNeil, S. Complications related to use of mesh implants in
- 532 surgical treatment of stress urinary incontinence and pelvic organ prolapse: infection or inflammation?
- 533 *World J. Urol.* **2019**.
- 534 31. Weisman, J.A.; Nicholson, J.C.; Tappa, K.; Jammalamadaka, U.; Wilson, C.G.; Mills, D.K. Antibiotic and
- 535 chemotherapeutic enhanced three-dimensional printer filaments and constructs for biomedical
- 536 applications. *Int. J. Nanomedicine* **2015**, *10*, 357–370.
- 537 32. Tappa, K.; Jammalamadaka, U.; Weisman, J.; Ballard, D.; Wolford, D.; Pascual-Garrido, C.; Wolford, L.;
- 538 Woodard, P.; Mills, D. 3D Printing Custom Bioactive and Absorbable Surgical Screws, Pins, and Bone

- 539 Plates for Localized Drug Delivery. *J. Funct. Biomater.* **2019**, *10*, 17.
- 540 33. Choi, Y.; Nirmala, R.; Lee, J.Y.; Rahman, M.; Hong, S.-T.; Kim, H.Y. Antibacterial ciprofloxacin HCl
541 incorporated polyurethane composite nanofibers via electrospinning for biomedical applications. *Ceram.*
542 *Int.* **2013**, *39*, 4937–4944.
- 543 34. Naik, A.D.; Fontaine, G.; Bellayer, S.; Bourbigot, S. Salen based Schiff bases to flame retard thermoplastic
544 polyurethane mimicking operational strategies of thermosetting resin. *RSC Adv.* **2015**, *5*, 48224–48235.
- 545 35. Punnakitikashem, P.; Truong, D.; Menon, J.U.; Nguyen, K.T.; Hong, Y. Electrospun biodegradable elastic
546 polyurethane scaffolds with dipyridamole release for small diameter vascular grafts. *Acta Biomater.* **2014**,
547 *10*, 4618–4628.
- 548 36. Siegel, A.L. Vaginal mesh extrusion associated with use of Mentor transobturator sling. *Urology* **2005**,
549 *66*, 995–999.
- 550 37. Genina, N.; Holländer, J.; Jukarainen, H.; Mäkilä, E.; Salonen, J.; Sandler, N. Ethylene vinyl acetate (EVA)
551 as a new drug carrier for 3D printed medical drug delivery devices. *Eur. J. Pharm. Sci.* **2016**, *90*, 53–63.
- 552 38. Ballard, D.H.; Weisman, J.A.; Jammalamadaka, U.; Tappa, K.; Alexander, J.S.; Griffen, F.D. Three-
553 dimensional printing of bioactive hernia meshes: In vitro proof of principle. *Surgery* **2017**, *161*, 1479–
554 1481.
- 555 39. Boyer, C.J.; Ballard, D.H.; Weisman, J.A.; Hurst, S.; McGee, D.J.; Mills, D.K.; Woerner, J.E.;
556 Jammalamadaka, U.; Tappa, K.; Alexander, J.S. Three-Dimensional Printing Antimicrobial and
557 Radiopaque Constructs. *3D Print. Addit. Manuf.* **2018**, *5*, 29–36.
- 558 40. CDC. Types of healthcare-associated infections. Healthcare-associated infections (HAIs) Available
559 online: <https://www.cdc.gov/HAI/infectionTypes.html> (accessed on Mar 10, 2019).
- 560 41. Khan, H.A.; Baig, F.K.; Mehboob, R. Nosocomial infections: Epidemiology, prevention, control and
561 surveillance. *Asian Pac. J. Trop. Biomed.* **2017**, *7*, 478–482.
- 562 42. Horan, T.C.; Andrus, M.; Dudeck, M.A. CDC/NHSN surveillance definition of health care–associated
563 infection and criteria for specific types of infections in the acute care setting. *Am. J. Infect. Control* **2008**,
564 *36*, 309–332.
- 565 43. Khan, H.A.; Ahmad, A.; Mehboob, R. Nosocomial infections and their control strategies. *Asian Pac. J.*
566 *Trop. Biomed.* **2015**, *5*, 509–514.
- 567 44. Lausch, K.R.; Fuursted, K.; Larsen, C.S.; Storgaard, M. Colonisation with multi-resistant
568 Enterobacteriaceae in hospitalised Danish patients with a history of recent travel: A cross-sectional
569 study. *Travel Med. Infect. Dis.* **2013**, *11*, 320–323.
- 570 45. Hall, C.W.; Mah, T.-F. Molecular mechanisms of biofilm-based antibiotic resistance and tolerance in
571 pathogenic bacteria. *FEMS Microbiol. Rev.* **2017**, *41*, 276–301.
- 572 46. Kollamaram, G.; Croker, D.M.; Walker, G.M.; Goyanes, A.; Basit, A.W.; Gaisford, S. Low temperature
573 fused deposition modeling (FDM) 3D printing of thermolabile drugs. *Int. J. Pharm.* **2018**, *545*, 144–152.
- 574 47. Goyanes, A.; Buanz, A.B.M.; Basit, A.W.; Gaisford, S. Fused-filament 3D printing (3DP) for fabrication
575 of tablets. *Int. J. Pharm.* **2014**, *476*, 88–92.
- 576 48. Ballard, D.H.; Jammalamadaka, U.; Tappa, K.; Weisman, J.A.; Boyer, C.J.; Alexander, J.S.; Woodard, P.K.
577 3D printing of surgical hernia meshes impregnated with contrast agents: in vitro proof of concept with
578 imaging characteristics on computed tomography. *3D Print. Med.* **2018**, *4*, 13.
- 579 49. Calero Castro, F.J.; Yuste, Y.; Pereira, S.; Garvín, M.D.; López García, M.Á.; Padillo, F.J.; Portilla, F. Proof
580 of concept, design, and manufacture via 3-D printing of a mesh with bactericidal capacity: Behaviour in
581 vitro and in vivo. *J. Tissue Eng. Regen. Med.* **2019**, *13*, 1955–1964.

- 582 50. Qamar, N.; Abbas, N.; Irfan, M.; Hussain, A.; Arshad, M.S.; Latif, S.; Mehmood, F.; Ghori, M.U.
583 Personalized 3D printed ciprofloxacin impregnated meshes for the management of hernia. *J. Drug Deliv.*
584 *Sci. Technol.* **2019**, *53*, 101164.
- 585 51. Statement by FDA Commissioner Scott Gottlieb, M.D., on FDA ushering in new era of 3D printing of
586 medical products; provides guidance to manufacturers of medical devices Available online:
587 [https://www.fda.gov/news-events/press-announcements/statement-fda-commissioner-scott-gottlieb-](https://www.fda.gov/news-events/press-announcements/statement-fda-commissioner-scott-gottlieb-md-fda-ushering-new-era-3d-printing-medical-products)
588 [md-fda-ushering-new-era-3d-printing-medical-products](https://www.fda.gov/news-events/press-announcements/statement-fda-commissioner-scott-gottlieb-md-fda-ushering-new-era-3d-printing-medical-products) (accessed on Mar 15, 2019).
589



© 2019 by the authors. Submitted for possible open access publication under the terms and conditions of the Creative Commons Attribution (CC BY) license (<http://creativecommons.org/licenses/by/4.0/>).

590